Localization and adiabatic pumping in a generalized Aubry-André-Harper model

Fangli Liu,* Somnath Ghosh, and Y. D. Chong†
School of Physical and Mathematical Sciences and Centre for Disruptive Photonic Technologies, Nanyang Technological University, Singapore 637371, Singapore

A generalization of the Aubry-André-Harper (AAH) model is developed, containing a tunable phase shift between on-site and off-diagonal modulations. A localization transition can be induced by varying just this phase, keeping all other model parameters constant. The complete localization phase diagram is obtained. Unlike the original AAH model, the generalized model can exhibit a transition between topologically trivial bandstructures and topologically non-trivial bandstructures containing protected boundary states. These boundary states can be pumped across the system by adiabatic variations in the phase shift parameter. The model can also be used to demonstrate the phenomenon of adiabatic pumping breakdown due to localization.

PACS numbers: 61.44.Fw, 42.25.Dd, 73.43.Cd

arXiv:1406.4675v3 [cond-mat.mes-hall] 1 Dec 2014

I. INTRODUCTION

The Aubry-André-Harper (AAH) model[1,2] is a workhorse for the study of localization and topological states in one dimension. It is described by[2]

$$t\left(\psi_{n+1}+\psi_{n-1}\right)+V_1\cos(Qn+k)\psi_n=E\psi_n, \quad (1)$$

where ψ_n is the wavefunction amplitude at site n, t is a nearest-neighbor hopping, and V_1, Q, and k are the amplitude, frequency, and phase of the on-site potential. The model emerges from the reduction of a two-dimensional (2D) Quantum Hall (QH) system to a one-dimensional (1D) chain, with k as the quasi-momentum transverse to the chain.[1,3] When the potential is made *quasiperiodic* by setting $Q/2\pi$ to an irrational number, the model has a localization transition[2–5]: all bulk eigenstates are extended for $0 < V_1 < 2t$, and localized for $V_1 > 2t$. The relationship between quasiperiodicity and localization has been explored in many subsequent variants of the model. Typically, altering the potential modulation leads to starkly different behaviors; some models exhibit mobility edges[2,6–8], while others lack any localization transition.[9] One important variant, which preserves the critical properties of the original AAH model, involves incommensurate modulations in the off-diagonal hopping coefficients.[10–13] In this case, all states are localized for $V_1 > 2\max(t, V_2)$, where V_2 is the amplitude of the off-diagonal modulation.[13]

Recently, the AAH model has attracted renewed attention[14–19], due to the realization that it can be implemented experimentally and used to study the topological properties of 2D bandstructures. In a pioneering paper, Kraus *et al.* demonstrated that an array of coupled optical waveguides can be used to realize a quasiperiodic AAH model with purely off-diagonal couplings, and that it is possible to implement a "topological pump" which adiabatically transfers boundary states across the array by winding the phase of the coupling modulations.[14] Interestingly, it has been shown that AAH models with on-site and/or off-diagonal modulation can be regarded as topologically equivalent to Fibonacci lattices of the same quasiperiodicity.[15,16] Madsen *et al.* have pointed out, however, that the boundary states occurring in these 1D lattices are not limited to the quasiperiodic case; they also appear in commensurate AAH models, and in both cases they can be explained by dimensional reduction from a topologically non-trivial 2D system.[17] For example, similar boundary states occur in the period-3 AAH model[18], and in the period-2 model the boundary states have Majorana-like characteristics.[19] However, incommensurate and commensurate AAH models do significantly differ in their localization properties.

This paper describes a generalization of the AAH model containing a tunable phase difference ϕ between the on-site and off-diagonal modulations. Previous studies of the AAH model have set $\phi = 0$, a condition that can be naturally derived from a 2D QH system with a uniform magnetic field.[10–13] However, this is an unnecessary restriction in experimental realizations like the coupled waveguide arrays described above; in these fabricated structures, the on-site potential and hopping amplitude can be independently controlled.

As we shall see, the generalized AAH model has several new and interesting behaviors which have not previously been explored. Firstly, in incommensurate lattices, a transition between purely extended and purely localized bulk states can be induced by varying ϕ, keeping the modulation amplitudes fixed. By contrast, in the original AAH model, localization can only be induced by varying the modulation amplitudes. Using a gauge argument, we are able to deduce the localization phase diagram for arbitrary ϕ. Secondly, the generalized AAH model can form topologically distinct families. As shown in Refs. 15,16, when AAH models are grouped by k (the phase common to both on-site and off-diagonal modulations), every bandgap in the E versus k bandstructure is topologically non-trivial but *equivalent*, regardless of other model parameters; topologically trivial bandgaps do not appear. However, when we use the *relative* phase ϕ as the pumping parameter, both types of bandgap can be observed for different parameter regimes. This allows us to propose a scheme for observing topological "phase transitions" using a family of 1D AAH models. Finally,

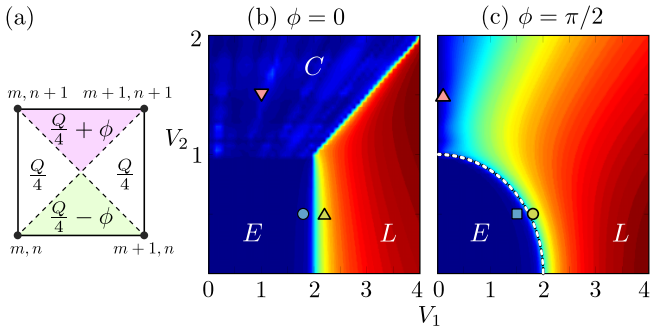

FIG. 1: (a) Distribution of magnetic flux in the unit cell which gives rise to the generalized AAH model of Eq. (2). (b,c) Localization phase diagrams for $\phi = 0$ and $\phi = \pi/2$, showing extended (E), localized (L), and critical (C) phases. The heat map shows the ground state's inverse participation ratio, with the largest values shown in red. The other parameters are $t = 1$, and $Q = (1 + \sqrt{5})\pi$. The dashed curve in (c) is the theoretical phase boundary, given by Eq. (10). The square, circle, and triangle symbols indicate the parameter choices for the plots in Fig. 2.

the model provides a convenient way to demonstrate an interesting property of topological pumps: the failure of pumping in the presence of localization, due to the breakdown of adiabaticity.[20–23]

II. MODEL

The generalized AAH model is described by the tight-binding equation

$$\begin{aligned}\left\{t + V_2 \cos\left[\left(n + \tfrac{1}{2}\right) Q + k\right]\right\} \psi_{n+1} \\ + \left\{t + V_2 \cos\left[\left(n - \tfrac{1}{2}\right) Q + k\right]\right\} \psi_{n-1} \\ + V_1 \cos(nQ + k + \phi)\psi_n = E\psi_n. \quad (2)\end{aligned}$$

The parameters t, V_1, Q, and k have the same meanings as in the original AAH model (1), and V_2 is the amplitude of the modulation in the off-diagonal hopping.[10–13] The on-site and off-diagonal modulations have the same wavenumber Q, but the latter has an additional phase ϕ.

Previous studies of the AAH model took $\phi = 0$, motivated by the derivation of the model from the dimensional reduction of a 2D QH system.[10–16] If the 2D system is assumed to have isotropic next-nearest-neighbor hoppings, and the magnetic vector potential is given by the Landau gauge $\vec{A} = Qy\hat{x}$ (corresponding to a uniform magnetic field with $Q/2\pi$ flux quanta per unit cell), the resulting 1D chains have the same frequency Q and phase k in the diagonal and off-diagonal modulations (i.e., $\phi = 0$).

However, the model of Eq. (2), with nonzero ϕ, can also be generated from a 2D QH system. The 2D system is simply required to have nonuniform magnetic flux, with the upper and lower quadrants of each unit cell receiving extra $\pm\phi$ flux respectively, as shown in Fig. 1(a). This can be described by a 2D Hamiltonian consisting of four separate terms:

$$H_1 = \sum_{mn} \frac{V_1}{2} e^{i(nQ+\phi)} a^\dagger_{m+1,n} a_{m,n} + \text{h.c.} \quad (3)$$

$$H_2 = \sum_{mn} t\, a^\dagger_{m,n+1} a_{m,n} + \text{h.c.} \quad (4)$$

$$H_3 = \sum_{mn} \frac{V_2}{2} e^{i(n+\frac{1}{2})Q} a^\dagger_{m+1,n+1} a_{m,n} + \text{h.c.} \quad (5)$$

$$H_4 = \sum_{mn} \frac{V_2}{2} e^{-i(n+\frac{1}{2})Q} a^\dagger_{m,n+1} a_{m+1,n} + \text{h.c.} \quad (6)$$

From the phases of the hopping coefficients, one can verify that the magnetic fluxes are as stated in Fig. 1(a). By Fourier transforming this Hamiltonian in the $+\hat{x}$ coordinate, we obtain $H = \sum_k \mathcal{H}(k)$, where k is the quasimomentum in the $+\hat{x}$ direction and $\mathcal{H}(k)$ is a 1D Hamiltonian corresponding to the tight-binding equation (2).

The redistribution of magnetic flux is reminiscent of Haldane's "zero field QH" model, which showed that the topological properties of a QH system can be altered without changing the net flux per unit cell.[24] In our model, the flux redistribution described by ϕ affects both the localization and topological properties of the 1D chains. Even though a 2D QH system with nonuniform flux may be challenging to implement, the 1D chains themselves can readily be realized, as will be discussed in Section V.

III. LOCALIZATION TRANSITION

For $\phi = 0$, the localization phase diagram was derived by Thouless and co-workers[12,13], and is shown in Fig. 1(b). For $V_1 > 2\max(t, V_2)$, all bulk eigenstates are localized; for $V_1, 2V_2 < 2t$, all bulk eigenstates are extended; and in the rest of the phase space, the eigenstates are critical.[13,25] The localization transition is driven by the amplitude of the modulations. In particular, for $V_2 < t$, localization only depends on V_1, and the critical value is the same as in the purely-diagonal AAH model.

Varying ϕ changes the phase diagram. As shown in Fig. 1(c), for $\phi = \pi/2$ the critical phase disappears, while the boundary between the extended and localized phases becomes an arc (which we will derive below). The heat maps in Fig. 1(b)–(c) show the ground state's inverse participation ratio (IPR) $\sum_n |\psi_n|^4$, which vanishes for extended states.[26]

Fig. 2 shows the ground state participation ratio (1/IPR) and probability density ($|\psi_n|^2$) for finite-size lattices with different choices of ϕ, V_1 and V_2. The ground states which are localized are easily identified in the $|\psi_n|^2$ versus n plots, as well as from the fact that the participation ratio remains constant with increasing system size N. For the extended states, the participation ratios scale linearly with N, as expected of 1D systems.[26] These results are in agreement with the phase diagrams plotted

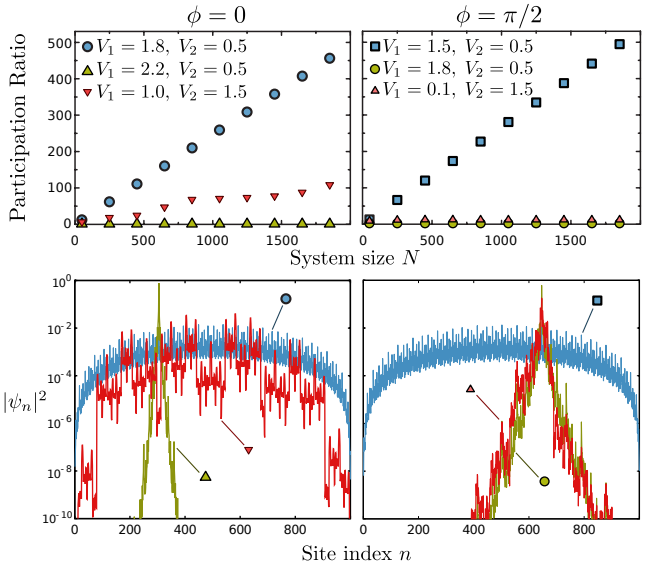
$\phi = 0$
$\phi = \pi/2$
Participation Ratio
$V_1 = 1.8,\ V_2 = 0.5$
$V_1 = 2.2,\ V_2 = 0.5$
$V_1 = 1.0,\ V_2 = 1.5$
$V_1 = 1.5,\ V_2 = 0.5$
$V_1 = 1.8,\ V_2 = 0.5$
$V_1 = 0.1,\ V_2 = 1.5$
System size N
$|\psi_n|^2$
Site index n

FIG. 2: (Color online) Ground state participation ratios and probability densities of the generalized AAH model, for $\phi = 0$ (left) and $\phi = \pi/2$ (right). The upper plots show the scaling of the ground state participation ratio $1/\sum_n |\psi_n|^4$ with system size N. The choice of V_1 and V_2 parameters is indicated by the matching symbols in the phase diagrams in Fig. 1; all other parameters are the same as in that figure. The lower plots show $|\psi_n|^2$ versus site index n for the ground states, for $N = 1000$ and the same parameters. The localized states have participation ratios that are constant in N, and are located in the localized region of the phase diagrams in Fig. 1.

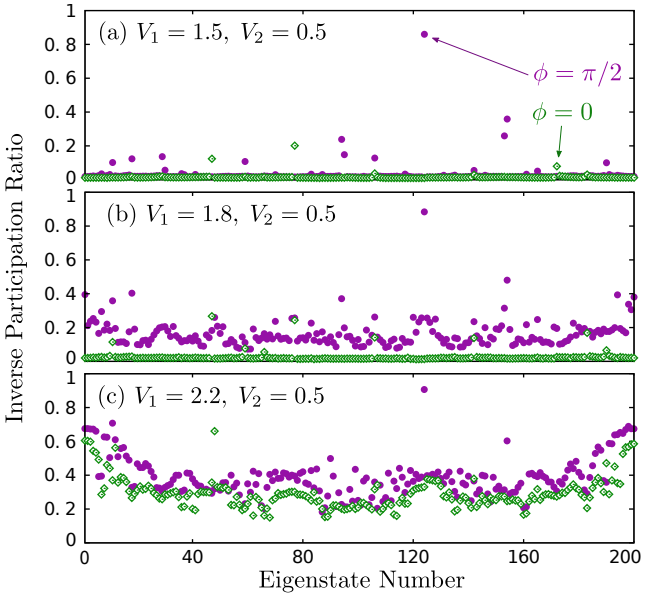

FIG. 3: (Color online) Inverse participation ratio (IPR) versus eigenvalue number for $V_2 = 0.5$ and (a) $V_1 = 1.5$, (b) $V_1 = 1.8$, and (c) $V_1 = 2.2$. Eigenstates are shown for $\phi = 0$ (green diamonds) and $\phi = \pi/2$ (magenta circles); the system size is $N = 200$, and all other parameters are the same as in Fig. 1. In (a), bulk states are extended for both values of ϕ; the states with large IPR turn out, upon inspection, to be boundary states. In (b), bulk states are extended for $\phi = 0$ and localized for $\phi = \pi/2$. In (c), the states are localized for both values of ϕ.

in Fig. 1(b)–(c). In particular, observe that for the parameter choice indicated by the yellow circles (right-hand plots of Fig. 2), the system is in the localized phase of the $\phi = \pi/2$ model; by contrast, for the same V_1 and V_2, the $\phi = 0$ model would be in the extended phase since $V_1 < 2t$. Furthermore, for the parameter choice indicated by the red upward-pointing triangles, the system is localized, whereas the $\phi = 0$ model would be critical.

Numerical results show that the excited states have the same localization properties as the ground states. Like the original AAH model, the generalized AAH model lacks a mobility edge. As demonstrated in Fig. 3, the bulk eigenstates are either all extended, or all localized regardless of the eigenstate energy. (In the finite lattice, however, localized *boundary* states can occur even in the extended phase, as discussed in the following sections.)

In the $\phi = 0$ AAH model, the localization behavior has long been understood to be tied to Aubry-André duality: the model is spectrally invariant under the exchange $t \leftrightarrow V_1/2$, which maps localized states to extended states and vice versa (and this remains true when off-diagonal modulations are included).[2,11–13]

The $\phi \neq 0$ model does *not* obey Aubry-André duality. Still, some of the analytic tractability of the original AAH model carries over to the generalized model. We take the QH system described by Eqs. (3)–(6), and apply the gauge transformation

$$\vec{A}_{mn} \to \vec{A}_{mn} - nQ\,\hat{x} + mQ\,\hat{y}. \tag{7}$$

Fourier transforming the 2D Hamiltonian in the $-\hat{y}$ coordinate then yields a 1D Hamiltonian corresponding to the following tight-binding equation:

$$\left\{\frac{V_1}{2}e^{i\phi} + V_2\,\cos\left[\left(m+\tfrac{1}{2}\right)Q + k'\right]\right\}\psi_{m+1} + \left\{\frac{V_1}{2}e^{-i\phi} + V_2\cos\left[\left(m-\tfrac{1}{2}\right)Q + k'\right]\right\}\psi_{m-1} + 2t\cos(mQ+k')\psi_m = E\psi_m. \tag{8}$$

Thus, the model is dual under a combination of exchanging $t \leftrightarrow V_1/2$, and moving the relative phase ϕ into the off-diagonal hopping term. Note that this reduces to the usual Aubry-André duality for $\phi = 0$.

We can deduce the localization phase boundary with the aid of Eq. (8), together with an argument due to Thouless.[12] The Thouless argument provides a lower bound for the measure of the spectrum; although originally given for the $\phi = 0$ case, it can be adapted to the model of Eq. (8) for $\phi \neq 0$, as shown in Appendix A. Using the principle that the measure of the spectrum vanishes at the localization transition[2,3], we find that the

localization phase boundary is described by

$$\sum_{\pm} \sqrt{(V_1/2)^2 \pm V_1 V_2 \cos\phi + V_2^2} = 2t. \tag{9}$$

For $\phi = 0$, Eq. (9) bounds a rectangular region $V_1 < 2t$, $V_2 < t$, which corresponds to the extended phase shown in Fig. 1(b); Aubry-André duality then implies the phase boundary $V_1 = 2\max(t, V_2)$, which describes the localized phase.[13] On the other hand, for $\phi = \pi/2$, Eq. (9) reduces to the semi-elliptical arc

$$(V_1/2)^2 + V_2^2 = t^2, \tag{10}$$

which agrees with the phase diagram shown in Fig. 1(c).

For intermediate values of ϕ, Eq. (9) is also in excellent agreement with numerical results, as shown in Figs. 7 and 8 in Appendix A. Furthermore, we find that the critical phase in the $\phi = 0$ phase diagram is unstable to variations in ϕ; for small $\phi \neq 0$, the entire region outside the extended phase consists of purely localized states.

IV. TOPOLOGICAL PROPERTIES

AAH models can be topologically characterized by noting that a family of AAH chains with different k's is essentially 2D, with k acting as an additional compact dimension. When Q is set to a rational approximant $2\pi q/p$, the 2D system has well-defined topological invariants in the form of the Chern numbers of the p bands[35]. Because the Chern fluxes are independent of k, V_1 and V_2 for $p \gg 1$, Kraus *et al.* argued that AAH models of the same Q can be regarded as being topologically equivalent and non-trivial.[14] In another work, it was shown that the AAH model can be continuously deformed into a Fibonacci quasicrystal[15]; this was confirmed by an optical lattice experiment showing that an AAH lattice and a Fibonacci lattice can be smoothly connected without closing the bulk gap.[16] In this context, topological transitions are only observed between AAH models with different modulation frequencies; for fixed Q, one cannot induce a topological transition in a manner similar to the localization transition, i.e. by varying the model parameters t, V_1, or V_2.

The generalized AAH model allows for a richer set of topological behaviors. If we use the phase ϕ as a winding parameter, instead of k, then the AAH model can exhibit *either* topological trivial *or* non-trivial bandstructures. We can also induce topological transitions between these two types of bandstructures by varying the model parameters.

It is important to note, at this point, that quasiperiodicity is not necessary for studying the topological properties of these 1D model families. As previous authors have noted, topological boundary states can appear in periodic and quasiperiodic systems alike.[17,18]

Fig. 4 shows the E versus ϕ bandstructures for the generalized AAH model. For a fixed lattice size $N = 50$,

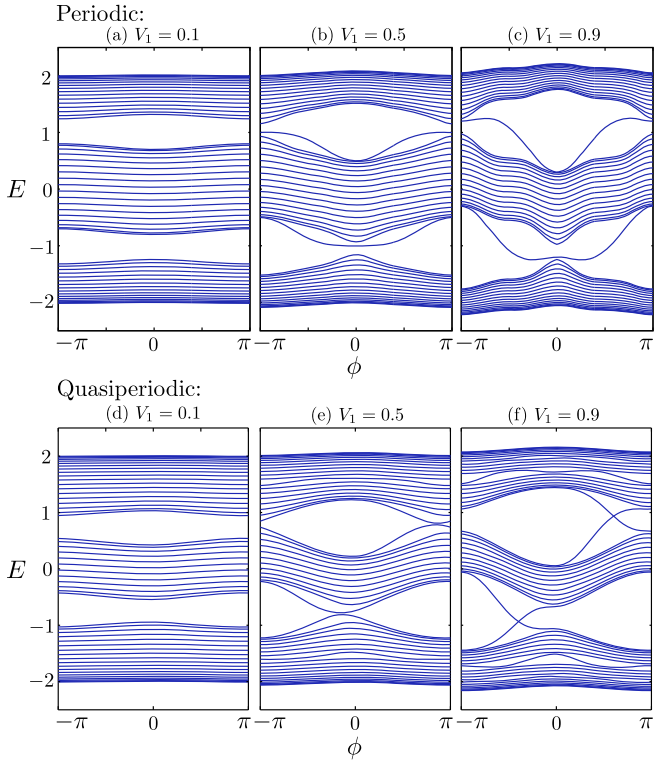

FIG. 4: (Color online) Bandstructures of E versus ϕ for the generalized AAH model. (a)–(c) Bandstructures of period-3 lattices ($Q = 10\pi/3$), for $V_1 = 0.1$, 0.5, and 0.9. (d)–(f) Bandstructures of quasiperiodic lattices ($Q = (1+\sqrt{5})\pi$), for those same values of V_1. The other model parameters are fixed at $V_2 = 0.25$, $t = 1$, $k = 0$, and $N = 50$.

two sets of results are shown: (i) period-3 lattices with $Q/2\pi = 5/3$, and (ii) quasiperiodic lattices with $Q/2\pi = (1+\sqrt{5})/2$. In both cases, the bandgaps are observed to be free of boundary states for small V_1; as V_1 is increased (with V_2 and other parameters fixed), the bulk bandgaps close and then re-open, and for large V_1 the re-opened gaps are spanned by boundary states. There is thus a transition from a topologically trivial phase to a non-trivial phase, for AAH chains of the *same* periodicity.

The topological nature of the boundary states can be demonstrated by adiabatically varying ϕ, similar to the adiabatic variation of k discussed in Ref. 14. In the topologically trivial phase, any boundary states that exist within the bandgaps (due to finite-size effects) are not topologically protected, and will remain confined to the same boundary as ϕ is varied. In the topological phase, however, boundary states that span the bandgaps, as shown in Fig. 4(c), are topologically protected, and varying ϕ pumps them across the chain.

To understand the topological transition, we study the period-3 model with $Q/2\pi = 5/3$. Its Bloch states are the eigenvectors of a 3×3 effective Hamiltonian which depends on ϕ and the quasimomentum along the chain. We can locate the gap closings, and within each gapped phase we can calculate the Chern numbers of the bands,

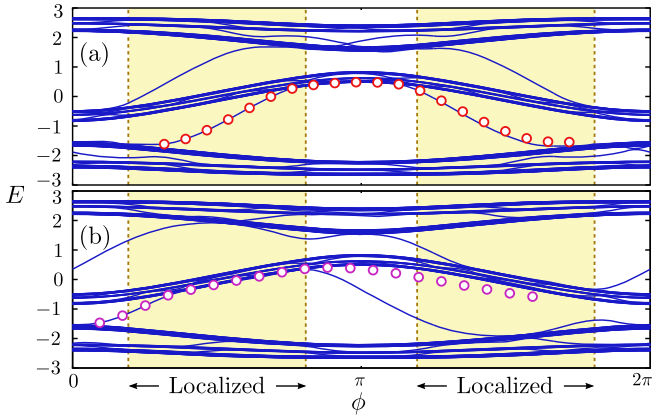

FIG. 5: (Color online) Bandstructures of E versus ϕ for (a) $k = 0$ and (b) $k = 0.3\pi$, with $V_1 = 1.9$, $V_2 = 0.5$, $t = 1$, $Q = (1+\sqrt{5})\pi$, and $N = 101$. Vertical dashes indicate the ϕ intervals over which the bulk states are localized. The red and purple circles show the expectation value $\langle\psi(t)|E|\psi(t)\rangle$, starting from a boundary state and taking $\phi(t) = 10^{-5}t$.

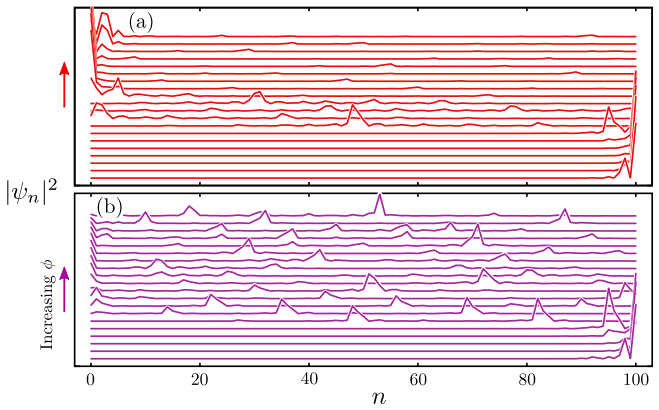

FIG. 6: (Color online) Plots of $|\psi_n|^2$ versus chain index n at subsequent times, based on numerical solutions of the time-dependent Schrödinger equation with a slowly-varying $\phi(\tau) = 10^{-5}\tau$. The other model parameters are the same as in Fig. 5, with (a) $k = 0$ and (b) $k = 0.3\pi$. Each $|\psi_n|^2$ plot corresponds to one of the circles in Fig. 5.

which characterize the topology of the bandstructure.[35] The details are given in Appendix B. The relevant topological phase boundary is found to occur along the curve

$$V_1 = \frac{V_2}{2}\left(\frac{4t - V_2}{t - V_2}\right). \tag{11}$$

As V_1 increases past the critical value, the bandstructure goes from topologically trivial, with Chern numbers $\{0, 0, 0\}$, to topologically nontrivial, with Chern numbers $\{-1, 2, -1\}$. For $V_1, V_2 \ll t$, the phase boundary occurs at approximately $V_1 \approx 2V_1$. This transition of the period-3 model appears to be a good match for the topological transition of the quasicrystal shown in Fig. 4(d)–(f).

V. DISCUSSION

The generalized AAH model is feasible to realize using optical waveguide lattices[27–29] or cold atom systems.[36] Such systems have been used to demonstrate Anderson localization in disordered lattices[30,31], localization in AAH chains[32,36], and adiabatic pumping of boundary states in off-diagonal AAH chains.[14] The rich physical behavior of the generalized AAH model motivates the implementation of simultaneous, independently-variable on-site and off-diagonal modulations in such experiments, so as to be able to tune the ϕ parameter.

In the context of optical waveguide lattices, for instance, the topological transition described in Section IV can be demonstrated using an array with two adjacent regions of the same Q but different t, V_1, and/or V_2. If the parameters are chosen so that the two regions are topologically distinct, then there will be some ϕ such that light injected at the interface is localized (due to overlap with a topological boundary state) rather than being scattered into the bulk. If the regions are topologically equivalent, the existence of boundary states will not be similarly guaranteed, but will instead depend sensitively on the parameter choices and interface conditions.

Optical lattices have been used extensively for studying the physics of localization, and the generalized AAH model provides an unusual opportunity to examine how localization affects the adiabatic pumping of topological boundary states. Pumping involves a boundary state adiabatically merging into a bulk band and becoming extended, then evolving into a boundary state at the opposite end.[14] However, this adiabatic process can break down when the bulk states become localized, due to the suppression of minimum level spacings in the localized regime.[20–23] This can be studied in a controlled way using the incommensurate generalized AAH model, since both localization and pumping are driven by the ϕ parameter. Fig. 5 shows a situation in which the bulk states are extended and localized at different values of ϕ. The parameter k changes the dispersion of the boundary states, though not the bulk bands; hence, we can use k to control whether a boundary state joins a band in the extended or localized regime. We simulate pumping by numerically solving $i\partial_\tau |\psi(\tau)\rangle = H[\phi(\tau)]\,|\psi(\tau)\rangle$, starting from a boundary state and increasing ϕ slowly (in the context of waveguide arrays, τ is the axial spatial coordinate[27]). Fig. 5(a) and Fig. 6(a) show successful pumping of a boundary state. For a different k (with $d\phi/d\tau$ and all other parameters kept the same), the boundary state merges into a localized bulk, and this causes the adiabatic pump to fail as shown in Fig. 5(b) and Fig. 6(b).

In summary, we have shown that a generalization of the AAH model has far-reaching implications for its localization and topological properties. These phenomena should be observable with existing experimental platforms. Features remaining to be explored include the fractal characteristics of the E versus ϕ bandstructures, and the robustness of the boundary states against disorder.

VI. ACKNOWLEDGMENTS

We thank M. Pasek, J. C. Pillay, M. C. Rechtsman, H. L. Wang, Y. Shikano, and Y. Y. Ma for their helpful comments. This research was supported by the Singapore National Research Foundation under grant No. NRFF2012-02, and by the Singapore MOE Academic Research Fund Tier 3 grant MOE-2011-T3-1-005.

Appendix A: Localization phase boundary

In this appendix, we adapt Thouless' derivation of a bound for the AAH model's spectral measure[12] to the generalized AAH model. This yields the localization phase boundary (9). As discussed in Section III, applying the gauge transformation (7) to the 2D Hamiltonian given by Eqs. (3)–(6) gives $H' = H'_1 + \cdots + H'_4$, where

$$H'_1 = \sum_{mn} \frac{V_1}{2} e^{i\phi}\, a^\dagger_{m+1,n} a_{m,n} + \text{h.c.} \tag{A1}$$

$$H'_2 = \sum_{mn} t\, e^{-imQ}\, a^\dagger_{m,n+1} a_{m,n} + \text{h.c.} \tag{A2}$$

$$H'_3 = \sum_{mn} \frac{V_2}{2} e^{-i(m+\frac{1}{2})Q} a^\dagger_{m+1,n+1} a_{m,n} + \text{h.c.} \tag{A3}$$

$$H'_4 = \sum_{mn} \frac{V_2}{2}\, e^{-i(m+\frac{1}{2})Q}\, a^\dagger_{m,n+1} a_{m+1,n} + \text{h.c.} \tag{A4}$$

Fourier transforming in $\hat{y}$ reduces H' to a family of 1D Hamiltonians $\mathcal{H}'(k')$ corresponding to Eq. (8).

We consider $Q = 2\pi q/p$, with $q, p \in \mathbb{Z}$ and p odd (which we write as $p = 2s+1$), and look for eigenstates of the infinite 1D chain satisfying

$$\psi_{m+p} = e^{ikp}\, \psi_m. \tag{A5}$$

(Note that ψ_m also depends implicitly on k'.) Due to gauge symmetry, the spectrum of $\mathcal{H}'(k')$ is independent of the phase of the hopping amplitudes, so we can replace Eq. (8) with the modified tight-binding equation

$$\mathcal{V}_{m-1,k'}\, \psi_{m-1} + 2t\cos(mQ + k')\psi_m + \mathcal{V}_{mk'}\, \psi_{m+1} = E\psi_m, \tag{A6}$$

where

$$\mathcal{V}_{mk'} \equiv \left| \frac{V_1}{2} e^{i\phi} + V_2 \cos\left[\left(m + \tfrac{1}{2}\right) Q + k'\right] \right|. \tag{A7}$$

To find a bound for the spectral measure, we focus on the high-symmetry points (i) $k = k' = 0$ and (ii) $k = \pi/p$, $k' = \pi$. For $k = 0, \pi/p$, the solutions can be split into those that are symmetric or antisymmetric about the points $m = 0$ and $m = s$. For the solutions that are symmetric about $m = 0$, we can define the variables $a_0 = \sqrt{2}\psi_0$ and $a_m = \psi_m + \psi_{-m} = 2\psi_m$ for $1 \le m \le s$. For both the $k' = 0$ and $k' = \pi$ cases, these satisfy:

$$2t\cos(k')\, a_0 + \sqrt{2}\mathcal{V}_{0k'}\, a_1 = E^{+\pm}\, a_0 \tag{A8}$$

$$\sqrt{2}\mathcal{V}_{0k'}\, a_0 + 2t\cos(Q + k')\, a_1 + \mathcal{V}_{1k'}\, a_2 = E^{+\pm} a_1 \tag{A9}$$

$$\mathcal{V}_{m-1,k'}\, a_{m-1} + 2t\cos(mQ + k')\, a_m + \mathcal{V}_{mk'}\, a_{m+1} = E^{+\pm}\, a_m \quad \text{for } 2 \le m < s \tag{A10}$$

$$\mathcal{V}_{s-1,k'}\, a_{s-1} + 2t\cos(sQ + k')\, a_s \pm \mathcal{V}_{sk'}\, a_s = E^{+\pm}\, a_s. \tag{A11}$$

The $\pm$ signs in these equations denote solutions that are symmetric about $p/2$ (for $k = 0$) and antisymmetric about $p/2$ (for $k = \pi/p$), respectively. These equations yield $s+1$ of the $2s+1$ eigenvalues of $\mathcal{H}'$.

The remaining s solutions are antisymmetric about $m = 0$. For these, let $b_0 = 0$ and $b_m = \psi_m - \psi_{-m} = 2\psi_m$. Then

$$\mathcal{V}_{m-1,k'}\, b_{m-1} + 2t\cos(mQ + k')\, b_m + \mathcal{V}_{mk'}\, b_{m+1} = E^{-\pm}\, b_m \quad \text{for } 1 \le m < s \tag{A12}$$

$$\mathcal{V}_{s-1,k'}\, b_{s-1} + 2t\cos(sQ + k')\, b_s \pm \mathcal{V}_{sk'}\, b_s = E^{-\pm} b_s, \tag{A13}$$

where the $\pm$ signs again denote solutions that are symmetric about $p/2$ (for $k = \pi$) and antisymmetric about $p/2$ (for $k = 0$).

For $k = k' = 0$, let us enumerate the eigenvalues of (A8)–(A13) by an index μ, in order of increasing energy. At this point, the eigenvalues of $\mathcal{H}'$ correspond to E^{++}_μ and E^{--}_μ, and the largest eigenvalue is E^{++}_{s+1}. By inspecting the structure of the tridiagonal matrix equations (A8)–(A11) and (A12)–(A13), one can derive the relations[12]

$$E^{--}_\mu, E^{++}_\mu \;<\; E^{-+}_\mu \;<\; E^{++}_{\mu+1}, \tag{A14}$$

$$\sum_{\mu=1}^{s} (E^{-+}_\mu - E^{--}_\mu) = 2\mathcal{V}_{s0} \tag{A15}$$

$$\sum_{\mu=1}^{s} \left(E^{-+}_\mu - E^{++}_\mu\right) = E^{++}_{s+1} - 2t. \tag{A16}$$

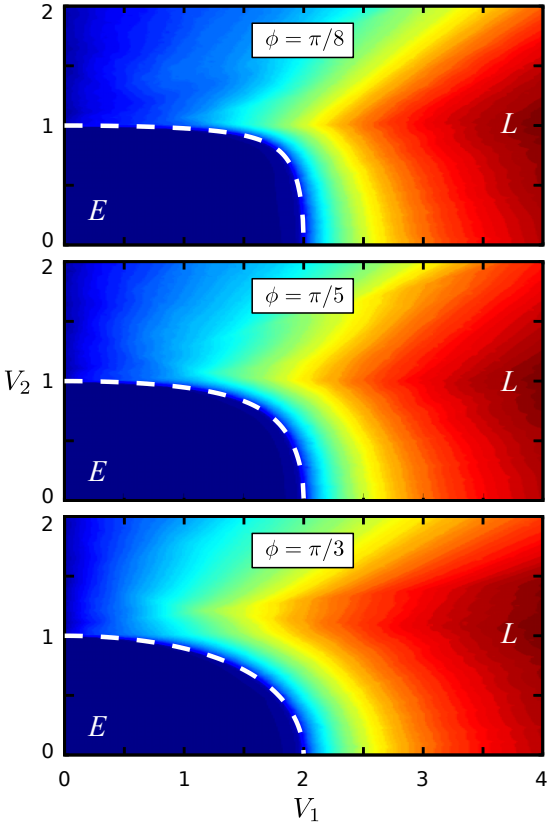

FIG. 7: Localization phase diagrams for $\phi = \pi/8$, $\phi = \pi/5$, and $\phi = \pi/3$, showing extended (E) and localized (L) phases of the generalized AAH model (2). The heat map shows the ground state's inverse participation ratio, with the largest values shown in red. The other parameters are $t = 1$ and $Q = (1+\sqrt{5})\pi$. The dashed curves show the theoretical phase boundary, given by Eq. (A20).

The bandgaps at $k = k' = 0$ lie between E_μ^{++} and E_μ^{--}, so using the above results we can derive the inequality

$$\begin{aligned}\sum_{\mu=1}^{s} &\left|E_\mu^{++} - E_\mu^{--}\right| \\ &\le \sum_{\mu=1}^{s} \left(\left|E_\mu^{++} - E_\mu^{-+}\right| + \left|E_\mu^{-+} - E_\mu^{--}\right| \right) \\ &= E_{s+1}^{++} + 2\mathcal{V}_{s0} - 2t.\end{aligned} \tag{A17}$$

Next, consider $k = \pi/p$ and $k' = \pi$. At this point, the eigenvalues of $\mathcal{H}'$ correspond to E^{+-} and E^{-+}. By inspecting Eqs. (A12)–(A13), we see that the E^{-+} eigenvalues are the negatives of the E^{--} eigenvalues which we would have calculated at $k = k' = 0$, except using hopping amplitudes $\mathcal{V}_{j\pi}$ instead of $\mathcal{V}_{j0}$. The other eigenvalues (E^{--}, E^{++}, and E^{--}) can all be mapped in a similar way. Under this mapping, the energies at the $k = \pi/p, k' = \pi$ point will be enumerated in *decreasing* order with μ, with E_{s+1}^{+-} being the lowest energy. The gaps lie between E_μ^{+-} and E_μ^{-+}, and the counterpart of (A17) under the mapping is:

$$\sum_{\mu=1}^{s} \left|E_\mu^{+-} - E_\mu^{-+}\right| \le -E_{s+1}^{+-} + 2\mathcal{V}_{s\pi} - 2t. \tag{A18}$$

The sum of the left-hand sides of (A17) and (A18) is an overestimate for the sum of the bandgaps of H' over the Brillouin zone.[12] The sum of the right-hand sides is

$$E_{s+1,k=k'=0}^{++} - E_{s+1,k=\pi/p,k'=\pi}^{+-} - 4t + 2\left(\mathcal{V}_{s0} + \mathcal{V}_{s\pi}\right),$$

where the first two terms constitute the energy difference between the top and bottom bands.

In the incommensurate limit, therefore, the measure of the spectrum is bounded below by

$$W_{\min} = 4t - 2\sum_{\pm} \left| \frac{V_1}{2} e^{i\phi} \pm V_2 \right|. \tag{A19}$$

From the principle that the measure vanishes at the localization transition[2,3], we deduce that the transition should occur when $W_{\min} = 0$; or, equivalently,

$$\sum_{\pm} \sqrt{(V_1/2)^2 \pm V_1 V_2 \cos\phi + V_2^2} = 2t. \tag{A20}$$

In Figs. 7 and 8, we compare this prediction for the phase boundary to the ground state inverse participation ratios calculated numerically from the tight-binding equation.[26] The results are in excellent agreement, and from this we conclude that the eigenstates of the generalized AAH model (2) are extended—and the eigenstates of the transformed models (8) and (A6) are localized—when

$$\sum_{\pm} \sqrt{(V_1/2)^2 \pm V_1 V_2 \cos\phi + V_2^2} < 2t. \tag{A21}$$

This also agrees well with the localization behaviors shown in Fig. 1, for the $\phi = 0$ and $\phi = \pi/2$ cases.

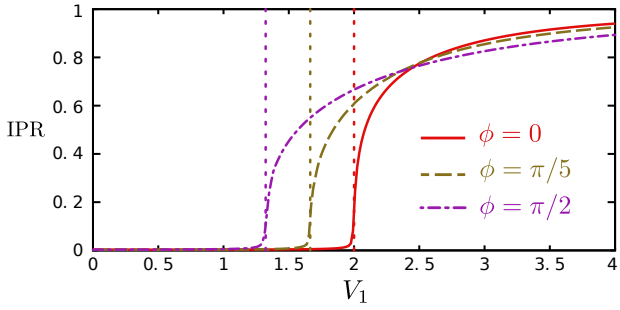

FIG. 8: (Color online) Ground state inverse participation ratio versus V_1, for the generalized AAH model (2), calculated using finite chains of length $N = 200$ with $V_2 = 0.75$, $t = 1$, and $Q = (1+\sqrt{5})\pi$, and three different values of ϕ. The vertical dashes show the phase boundaries predicted by Eq. (A20).

Appendix B: The period-3 generalized AAH model

As Madsen *et al.* have recently emphasized, there is no essential difference in the way quasicrystals and ordinary crystalline lattices are topologically classified.[17] In order to understand the topological properties of the generalized AAH model (2), it is sufficient to study rational values of $Q/2\pi$. This is equivalent to taking a "magnetic unit cell" of the 2D quantum Hall lattice.[35]

In most of our numerical examples, we have set $Q/2\pi$ to the golden ratio $(1+\sqrt{5})/2 = 1.61803\ldots$, which is a conventional choice for 1D quasicrystals. To understand the resulting topological properties, however, we have found it convenient to study a period-3 lattice with $Q/2\pi = 5/3 = 1.666\ldots$ (a truncation of the golden ratio's continued fraction). As shown in Fig. 4, it accounts well for the two complete bandgaps observed in the quasicrystal, as well as the existence of topological edge states. The period-3 model has several interesting properties, which are summarized in this Appendix.

Consider an infinite chain with $k = 0$. Bloch wavefunctions satisfy $\psi_{n+3} = e^{iK}\psi_n$, where $K \in [0, 2\pi)$ denotes the quasi-momentum along the 1D chain. Eq. (2) reduces to a eigenvalue problem $\mathcal{H}(\phi, K)\psi = E\psi$, where $\psi \equiv [\psi_{n-1}, \psi_n, \psi_{n+1}]^T$, and

$$\mathcal{H}(\phi,K) = \begin{bmatrix} V_1\cos(-Q+\phi) & \alpha & \beta\, e^{-iK} \\ \alpha & V_1\cos(\phi) & \alpha \\ \beta\, e^{iK} & \alpha & V_1\cos(Q+\phi) \end{bmatrix}, \tag{B1}$$

where

$$\alpha \equiv t + V_2\cos(Q/2)$$
$$\beta \equiv t + V_2\cos(3Q/2).$$

This Hamiltonian depends parametrically on K and ϕ. Although ϕ lacks a straightforward interpretation as a quasi-momentum, we can nonetheless treat the parameter space spanned by $K, \phi \in [0,\ 2\pi]$ as an abstract "Brillouin zone". The Hamiltonian obeys the symmetries

$$\mathcal{H}(\phi,K) \;=\; \mathcal{H}(\phi,-K)^* \;=\; \Gamma\mathcal{H}(-\phi,-K)\Gamma, \tag{B2}$$

where

$$\Gamma = \begin{bmatrix} 0 & 0 & 1 \\ 0 & 1 & 0 \\ 1 & 0 & 0 \end{bmatrix}. \tag{B3}$$

We can diagonalize $\mathcal{H}(\phi, K)$ for many discrete values of $K \in [0, 2\pi)$ to produce a "projected bandstructure" of E versus ϕ. Alternatively, for a finite chain of length $N \gg 1$, the energy levels can be obtained directly from Eq. (2), which yields bandstructures like those shown in Fig. 4. These finite-system bandstructures, unlike the ones obtained from diagonalizing $\mathcal{H}(\phi, K)$, can contain dispersion curves corresponding to topological boundary states. For fixed V_2, we observe that when V_1 is sufficiently small, the bandstructures appear to be topologically trivial, i.e. there are no boundary states in either bandgap, as shown in Fig. 4(a). For large V_1, the bandstructure is topologically non-trivial, as in Fig. 4(c).

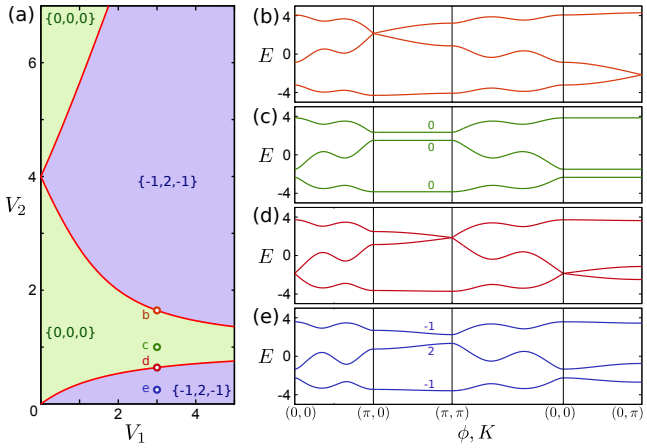

FIG. 9: (Color online) (a) Topological phase diagram of the period-3 AAH model. The phase boundaries are given by Eqs. (B7)–(B9), and labels indicate the bands' Chern numbers. (b)–(e) Band diagrams at the values of V_1 and V_2 indicated in (a): (b) $V_1 = 3, V_2 = 1.6458$; (c) $V_1 = 3, V_2 = 1$; (d) $V_1 = 3, V_2 = 0.64110$; (d) $V_1 = 3, V_2 = 0.25$. The gapped bands are labeled by their Chern numbers. The other parameters are $t = 1$, $Q = 10\pi/3$, and $k = 0$.

In order to understand the topological phase diagram quantitatively, we look for bandgap closings in the bulk Hamiltonian $\mathcal{H}(\phi, K)$. The symmetry relations (B2) indicate that we can focus on the high-symmetry points in the Brillouin zone: $(0,0)$, (π,π), $(\pi,0)$, and $(0,\pi)$. At these points, the Hamiltonian has another important property, which can be seen from the matrix structure of Eq. (B1): the eigenvalues of $\mathcal{H}(0,0)$ are the negatives of the eigenvalues of $\mathcal{H}(\pi,\pi)$, and the eigenvalues of $\mathcal{H}(0,\pi)$ are the negatives of the eigenvalues of $\mathcal{H}(\pi,0)$. As a result, bandgap closings always occur in pairs, at different points in the Brillouin zone. But, unlike familiar cases such as graphene, these simultaneous pairwise closings occur at different energies, in different bandgaps.

By diagonalizing $\mathcal{H}(0,0)$, we obtain the eigenvalues

$$\mathcal{E}_0 = -t + V_1\cos(Q) - V_2\cos(3Q/2)$$
$$\mathcal{E}_\pm = \frac{Z \pm W}{2}, \tag{B4}$$

where

$$Z = t + V_1 + V_1\cos(Q) + V_2\cos(3Q/2) \tag{B5}$$
$$W^2 = Z^2 + 8\Big[t + V_2\cos(Q/2)\Big]^2 - 4V_1\Big[t + V_1\cos(Q) + V_2\cos(3Q/2)\Big]. \tag{B6}$$

We now set $Q = 10\pi/3$ for specificity. The bandgaps at $(0,0)$ and (π,π) close when $\mathcal{E}_0 = \mathcal{E}_\pm$; this yields the phase boundaries

$$V_2 = 2t + V_1 \pm \sqrt{(t+V_1)^2 + 3t^2}, \tag{B7}$$

or, equivalently,

$$V_1 = \frac{V_2}{2}\left(\frac{4t - V_2}{t - V_2}\right). \tag{B8}$$

Next, consider $\mathcal{H}(0,\pi)$. Following a similar procedure, we find that the bandgaps at $(0,\pi)$ and $(\pi,0)$ close when

$$V_2 = 2t - V_1 + \sqrt{(t-V_1)^2 + 3t^2}. \tag{B9}$$

(The $-$ solution is discarded since it gives negative V_2; by convention, the modulation amplitudes are positive.)

As shown in Fig. 9(a), Eqs. (B7) and (B9) partition the $\{V_1, V_2\}$ phase space into four distinct gapped phases. We can characterize the topology of the gapped bandstructures by calculating each band's Chern number,[35]

$$C_n = \frac{1}{2\pi i}\int\!\!\int_{BZ} d\phi\, dK \left(\frac{\partial A^K_{nn}}{\partial \phi} - \frac{\partial A^\phi_{nn}}{\partial K}\right), \tag{B10}$$

$$\vec{A}_{nn'} = \left\langle n, \phi, K \middle| \vec{\nabla}_{\phi,K} \middle| n', \phi, K \right\rangle. \tag{B11}$$

Here, $|n, \phi, K\rangle$ denotes the Bloch eigenstate in the nth band at parameter values (ϕ, K). As indicated in Fig. 9(a), the topologically trivial bandstructures have Chern numbers $\{0,0,0\}$, while the topologically nontrivial bandstructures have Chern numbers $\{-1,2,-1\}$.

The bottom-most phase boundary in Fig. 9(a), which corresponds to the $-$ solution of Eq. (B7), cuts across the localization phase boundary of the incommensurate generalized AAH model (see Figs. 1 and 7). When the incommensurate model is in the extended phase, or not too deep into the localized phase, we find that its topological behavior closely matches the behavior of the period-3 model. Specifically, its bandstructure contains two primary complete bandgaps, which occur at energies similar to the bandgaps of the period-3 model and have similar topological transitions, as shown in Figs. 4 and 5. This correspondence appears to break down, however, deep in the localized phase. Future studies will seek a better understanding of the incommensurate model's topological properties within the strongly localized regime.

* Electronic address: liuf0025@e.ntu.edu.sg
† Electronic address: yidong@ntu.edu.sg

[1] P. G. Harper, Proc. Phys. Soc. Lond. **A68**, 874 (1955).
[2] S. Aubry and C. André, Proc. Israel Phys. Soc. **3**, 133 (1980).
[3] D. R. Hofstadter, Phys. Rev. B **14**, 2239 (1976).
[4] S. Y. Jitomirskaya, Ann. Math. **150**, 1159 (1999).
[5] B. Simon, Adv. Appl. Math. **3** 463 (1982).
[6] C. M. Soukoulis and E. N. Economou, Phys. Rev. Lett. **48**, 1043 (1982).
[7] H. Hiramoto and M. Kohmoto, Phys. Rev. Lett. **62**, 2714 (1989).
[8] J. Biddle, B. Wang, D. J. Priour, Jr., and S. Das Sarma, Phys. Rev. A **80**, 021603(R) (2009).
[9] D. R. Grempel, S. Fishman, R. E. Prange, Phys. Rev. Lett. **49**, 833 (1982).
[10] F. H. Claro and G. H. Wannier, Phys. Rev. B **19**, 6068 (1979).
[11] Y. Hatsugai and M. Kohmoto, Phys. Rev. B **42**, 8282 (1990).
[12] D. J. Thouless, Phys. Rev. B **28**, 4272 (1983).
[13] J. H. Han, D. J. Thouless, H. Hiramoto, and M. Kohmoto, Phys. Rev. B **50**, 11365 (1994).
[14] Y. E. Kraus, Y. Lahini, Z. Ringel, M. Verbin, and O. Zilberberg, Phys. Rev. Lett. **109**, 106402 (2012).
[15] Y. E. Kraus and O. Zilberberg, Phys. Rev. Lett. **111**, 116404 (2012).
[16] M. Verbin, O. Zilberberg, Y. E. Kraus, Y. Lahini, and Y. Silberberg, Phys. Rev. Lett. **110**, 076403 (2013).
[17] K. A. Madsen, E. J. Bergholtz, and P. W. Brouwer, Phys. Rev. B. **88**, 125118 (2013).
[18] L. J. Lang, X. Cai, and S. Chen, Phys. Rev. Lett **108** 220401 (2012).
[19] S. Ganeshan, K. Sun, and S. Das Sarma, Phys. Rev. Lett. **110**, 180403 (2013).
[20] S. A. Molcanov, Commun. Math. Phys. **78**, 429 (1981).
[21] M. Feingold, S. Fishman, D. R. Grempel, and R. E. Prange, Phys. Rev. **B** 31, 6852 (1985).
[22] S. Jansen, M. B. Ruskai and R. Seiler, J. Math. Phys. **48**, 102111 (2007).
[23] B. Altshuler, H. Krovi, and J. Roland, Prod. Nat. Acad. Sci. **107**, 12446 (2010).
[24] F. D. M. Haldane, Phys. Rev. Lett. **61**, 2015 (1988).
[25] I. Chang, K. Ikezawa and M. Kohmoto, Phys. Rev. B **55**, 12971 (1997).
[26] D. J. Thouless, Phys. Rep. **13**, 93 (1974).
[27] H. De Raedt, A. Lagendijk, and P. de Vries, Phys. Rev. Lett. **62**, 47 (1989).
[28] D. N. Christodoulides, F. Lederer, and Y. Silberberg, Nature (London) **424**, 817 (2003).
[29] T. Pertsch *et al.*, Phys. Rev. Lett. **93**, 053901 (2004).
[30] T. Schwartz, G. Bartal, S. Fishman, and M. Segev, Nature (London) **446**, 52 (2007).
[31] Y. Lahini, A. Avidan, F. Pozzi, M. Sorel, R. Morandotti, D. N. Christodoulides, and Y. Silberberg, Phys. Rev. Lett. **100**, 013906 (2008).
[32] Y. Lahini, R. Pugatch, F. Pozzi, M. Sorel, R. Morandotti, N. Davidson, and Y. Silberberg, Phys. Rev. Lett. **103**, 013901 (2009).
[33] L. Martin *et al.*, Opt. Ex. **19**, 13636 (2011).
[34] S. Ghosh, N. D. Psaila, R. R. Thomson, B. P. Pal, R. K. Varshney, and A. K. Kar, Appl. Phys. Lett. 100, 101102 (2012).
[35] D. Thouless, M. Kohmoto, M. P. Nightingale, and M. den Nijs, Phys. Rev. Lett. **49**, 405 (1982).
[36] G. Roati *et al.*, Nature (London) **453**, 895 (2008).